Evaluation of different Ni/Al_2O_3 catalysts in glycerol steam reforming for hydrogen production

João Paulo da S. Q. Menezes, Flávia da C. Jácome, Robinson L. Manfro and Mariana M. V. M. Souza*

Escola de Química- Universidade Federal do Rio de Janeiro (UFRJ), Centro de Tecnologia, Bloco E, sala 206, CEP 21941-909, Rio de Janeiro, RJ, Brazil.

*Corresponding author (Phone: 55-21-39387598, E-mail: mmattos@eq.ufrj.br)

Abstract

Biodiesel production by transesterification has grown worldwide, as also the glycerol produced as a byproduct, which has accumulated in the market, waiting for an adequate disposal. Thus, hydrogen production by glycerol steam reforming is an attractive alternative, as it represents the conversion of a waste in a high-added value product. In this work, three catalysts were synthesized by wet impregnation of nickel precursor in different supports: γ-Al_2O_3 prepared by boehmite calcination, α-Al_2O_3 and 15% wt. CaO-γAl_2O_3 prepared by wet impregnation of calcium oxide precursor in γ-Al_2O_3. A commercial catalyst for methane steam reforming (Ni/CaO-Al_2O_3) was also evaluated. The catalysts were characterized by XRF, XRD, BET, TPR, TPD-NH_3, TGA and DTA. Catalytic tests were performed at 500 ºC, glycerol feed of 20% v/v and GHSV of 200,000 h^{-1}. The calcium oxide incorporation reduced the formation of nickel aluminate phase ($NiAl_2O_4$) and the amount and strength of catalyst acidity. Furthermore, it was the only catalyst that has not presented deactivation in 30 h of reaction, showing the highest glycerol conversion and hydrogen yield after 24 h of reaction. Ni-γAl_2O_3 and Ni-αAl_2O_3 have presented a severe deactivation, which was associated with coke formation. The synthesized catalysts presented better catalytic performance for glycerol steam reforming in comparison with commercial catalyst, in terms of higher glycerol conversion, glycerol conversion to gas and hydrogen yield.

Keywords: glycerol, reforming, hydrogen, nickel, alumina.

1. Introduction

Fossil fuels have supplied most of the world energy along decades, playing an essential role in developing many sectors of economy. However, these resources are non-renewable and its extensive use is related to pollutant gases emission, especially gases associated with global warming. Thus, considering the increasing concern about environmental issues, there is an urgent demand in gradually incorporate biofuels, as biodiesel and ethanol, in current energy supply matrix [1].

Biodiesel is mostly produced by oil/fat transesterification and Brazil is one of the pioneers in its production and use. Currently, ANP (Brazilian Agency for Petroleum, Natural Gas and Biofuels) stipulates the addition of 8% biodiesel in diesel, which has grown biodiesel production in the country. However, biodiesel production by transesterification generates glycerol as a byproduct, as 100 kg of glycerol is produced for each ton of biodiesel produced [2]. This produced glycerol has lots of impurities like the catalyst, alcohols, fatty acids, salts and water, thus its direct use in usual applications, as pharmaceutical, cleaning and food industries, which require a high level of purity, is impracticable. Therefore, developing a new route for glycerol conversion into high-added value products would not only solve the problem of glycerol disposal, but would also contribute for turning biodiesel production more competitive towards diesel production. In this context, the hydrogen production by glycerol steam reforming must be highlighted.

Hydrogen is the most abundant molecule in the world and its use in chemical industries is indispensable. For instance, hydrogen is employed for ammonia and methanol production, for oil refining in hydrodesulfurization and hydrocracking processes and for Fischer-Tropsch synthesis. Furthermore, hydrogen is considered a clean fuel, as its application in fuel cells does not release significant amount of pollutant gases. However, most of hydrogen production currently is through natural gas (48%), heavy oils (30%) and coal (17%). Only a small part of the production is provided by water electrolysis (4%) or by biomass derivatives (1%) [3]. The study of glycerol conversion into hydrogen also intends to increase the participation of green resources in the hydrogen production matrix.

Glycerol steam reforming consists in reaction of glycerol with steam for producing synthesis gas (hydrogen and carbon monoxide) at atmospheric pressure and temperatures above 500 ºC. Shift reaction (Eq.1) occurs next and consists in CO reaction with steam for producing more hydrogen and CO_2. Shift reaction is exothermic, however the global reforming reaction (Eq.2) is endothermic [4].

$$CO + H_2O \leftrightarrow CO_2 + H_2 \quad (1)$$

$$C_3H_8O_3 + 3H_2O \leftrightarrow 7H_2 + 3CO \quad (2)$$

One advantage of glycerol steam reforming over methane steam reforming is the higher hydrogen yield; for one mole of glycerol feed, seven hydrogen moles can be produced, while only three moles of hydrogen by one mole feed of methane. Furthermore, methane reforming represents a fuel consumption for producing hydrogen, which is not true for glycerol reforming [5]. Beyond that, methane reforming takes place at 700-1000 ºC, while glycerol steam reforming takes place at lower temperatures.

The development of a suitable catalyst for glycerol steam reforming with good properties as stability, high dispersion of active phase, low coke and byproduct formation and high hydrogen yield, is a subject that needs investigation and further improvements. A good catalyst for glycerol reforming has to be active for the cleavage of C-C bonds and water gas shift reaction. However, it has to inhibit the cleavage of C-O bonds and methane formation [6–9]. Catalysts based on noble metals are less susceptible to deactivation through coke deposition and more active for reforming reaction. However, these catalysts are expensive and their availability is limited, thus it is more economical the development of catalysts based on non-noble metals, as nickel, which presents high activity for C-C bond scission and selectivity for synthesis gas production [9].

γ-Alumina is the most employed support in steam reforming catalysts, because of its high surface area that leads to a good dispersion of the active phase. However, many authors have reported high coke formation on γ-alumina catalysts that causes catalyst deactivation. Silva et al. [5] suggest that coke formation occurs in γ-alumina acid sites due to dehydration, cracking and polymerization reactions. Thus, in this work, nickel catalysts with different alumina supports were evaluated in glycerol steam reforming, including CaO incorporation on γ-alumina, in order to reduce catalyst acidity and coke formation.

2. Experimental

2.1. Catalyst preparation

Three catalysts were synthesized by wet impregnation of 20 wt.% nickel precursor ($Ni(NO_3)_2.6H_2O$ - Vetec) on three different supports: γ-Al_2O_3 synthesized by boehmite (Sasol)

calcination at 500 ºC in air flow (60 $mLmin^{-1}$), commercial α-Al_2O_3 and 15% wt. CaO-Al_2O_3 synthesized by wet impregnation of calcium oxide precursor ($Ca(NO_3)_2.4H_2O$) on γ-Al_2O_3 support followed by calcination at 500 ºC with air (60 $mLmin^{-1}$). The catalysts were dried at 100 ºC overnight and calcined at 500 ºC with air (60 $mLmin^{-1}$) for converting nickel nitrate into nickel oxide. The catalysts will be referred to as Ni-γAl, Ni-αAl and NiCaAl, respectively.

A fourth catalyst of Ni/CaO-Al_2O_3 (15% NiO and 14% CaO) used for commercial methane steam reforming was also evaluated for comparison and will be referred to as NiCaAlcom.

2.2. Catalyst characterization

The chemical composition of the catalysts was analyzed by X-ray fluorescence (XRF) using a Rigaku Primini spectrometer.

The textural properties of the catalysts were determined by N_2 adsorption-desorption at -196 °C in a Micromeritics TriStar 3000. The BET method was utilized for specific area calculation and BJH method for pore volume determination. Prior to the analysis the samples were outgassed for 24 h at 300 °C.

X-ray powder diffraction (XRD) patterns were recorded in a Rigaku Miniflex II X-ray diffractometer equipped with a graphite monochromator using CuKα radiation (30 kV and 15 mA). The analysis were carried out with a step of 0.05°, counting time of 1 second for step and over a 2θ range of 5° to 90°. Reduced catalysts were analyzed after ex-situ reduction at the same conditions used before the catalytic tests and spent catalysts were analyzed without any other treatment after reaction. The Ni average crystallite size was calculated by Scherrer equation, using the peak at 44.5°, correspondent to the most intense Ni peak. Ni dispersion of the catalysts was estimated according to Anderson (Eq.3) [10].

$$D = \frac{6.Vm}{d.Am} \quad (3)$$

where Vm is the Ni atomic volume (0.0109 nm^3), d is the crystallite size (nm) and Am is the surface area of a single nickel atom (0.0649 nm^2).

The reduction profile and reducibility of the catalysts were analyzed by temperature-programmed reduction (TPR). This analysis was carried out in a microflow reactor at atmosphere

pressure. Approximately 50 mg of the samples were firstly treated at 150 °C under 30 $mLmin^{-1}$ of argon. After the pretreatment, the reduction was carried out up to 1000 °C with a heating rate of 10 $°Cmin^{-1}$ under 30 $mLmin^{-1}$ of a mixture 1.8% H_2/Ar. The hydrogen consumption was monitored using a thermal conductivity detector (TCD).

The catalyst acidity was analyzed by temperature programmed desorption of ammonia (TPD-NH_3) using a Pfeifer QMG-220 mass spectrometer mass spectrometer to register the ammonia consumption. The samples were firstly reduced with a mixture 1.8% H_2/Ar (30 $mLmin^{-1}$) at 800 °C with a heating rate of 10 $°Cmin^{-1}$ and remaining at this temperature for 30 min. After the reduction, the ammonia adsorption was performed at 70 °C for 30 min using a mixture of 4 % NH_3/He, and then the physisorbed ammonia was removed with He flow of 30 $mLmin^{-1}$. The chemisorbed ammonia desorption was carried out up to 800 °C with a rate of 20 $°Cmin^{-1}$ and remaining at this temperature for 30 min. The ratio m/z =15 was used for ammonia quantification.

The quantification of coke deposition in spent catalysts was performed by thermogravimetric analysis (TGA) and differential thermal analysis (DTA) with a TA SDT Q600 equipment. The analysis was carried out up to 1000 °C with a rate of 10 $°Cmin^{-1}$ under a synthetic air flow of 50 $mLmin^{-1}$ and the mass sample in each analysis was between 3 and 10 mg.

The morphology of the catalysts after calcination and after reaction was analyzed by scanning electron microscopy (SEM), with a Hitachi TM-3030 microscope. The acceleration voltage was 15 kV, using backscattering electron.

2.3. Catalytic tests

The glycerol steam reforming reaction was carried out in a fixed bed reactor of quartz at 500 °C and atmospheric pressure. The catalysts were reduced in situ under 30% H_2/N_2 flow (90 $mLmin^{-1}$) up to 800 °C at a heating rate of 10 $°Cmin^{-1}$ and remaining at this temperature for 30 min. The reduction temperature was chosen based on the reduction profiles (TPR) of the catalysts. The gas hourly space velocity (GHSV) employed was 200,000 h^{-1}. The aqueous solution of glycerol (20 % v/v), which represents a water:glycerol molar ratio of 16.2, was injected to the reactor by a pump (Eldex 1SAM), with flow rate of 0.106 $mLmin^{-1}$. The vaporization of the solution was conducted in a vaporizer at 225 °C

under He flow as a diluent; the He flow was calculated for being 20 % v/v of the total gas flow (250 $mLmin^{-1}$).

The diffusional test was conducted in order to ensure that data collected were at kinetic regime. The mass chosen for the catalytic tests was 150 mg of catalyst. The catalysts were diluted with silicon carbide in a mass proportion of 1:5 (catalyst:silicon carbide).

The gas products of the reaction passed through a heat exchanger at 10 °C in order to separate the liquid phase from the gas phase. The gas phase was analyzed online by a gas chromatograph (GC) Shimadzu GC-2014 equipped with two columns (RT-QPLOT and Carboxen 1010) and thermal conductivity (TCD) and flame ionization (FID) detectors. The liquid phase was analyzed by high-performance liquid chromatography (HPLC) Shimadzu Prominence with a Bio-Rad Aminex HPX-87H column, using 0.01 M H_2SO_4 as eluent at 0.6 $mLmin^{-1}$, and with UV and refractive index detectors.

The catalyst performance was evaluated according to the following equations:

- Glycerol conversion (Eq.4):

$$X\,(\%) = \frac{N^{In}_{Glycerol}(mol\ h^{-1}) - N^{Out}_{Glycerol}(mol\ h^{-1})}{N^{In}_{Glycerol}(mol\ h^{-1})}\,.100 \quad (4)$$

- Glycerol conversion into gas (Eq.5):

$$X_G\,(\%) = \frac{\text{C moles in gas products}}{\text{C moles in feed}}.100 \quad (5)$$

- Yield of a liquid byproduct (Eq.6):

$$Y_i\,(\%) = \frac{N^{Out}_{i}(mol\ h^{-1})}{N^{In}_{Glycerol}(mol\ h^{-1})}\,.100 \quad (6)$$

where "i" refers to acrolein, acetol or propanoic acid.

- Hydrogen yield (Eq.7):

$$Y_{H_2}(\%) = \frac{N^{Out}_{H_2}(mol\ h^{-1})}{7N^{In}_{Glycerol}(mol\ h^{-1})}.100 \quad (7)$$

- Selectivity to hydrogen (Eq.8):

$$S_{H_2}(\%) = \frac{\text{Molecules of } H_2 \text{ produced}}{\text{C atoms in gas product}}.\frac{1}{RR}.100 \quad (8)$$

where RR is the H_2/CO_2 reforming ratio of 7/3 for glycerol.

- CO, CO_2, and CH_4 selectivities (Eq.9):

$$S_i(\%) = \frac{\text{C moles in specie i}}{\text{C moles in gaseous products}} . 100 \quad (9)$$

where i species are CO, CO_2 and CH_4.

- Hydrogen production rate (Eq.10):

$$H_2 \text{ production rate} \left(\frac{\mu mol}{gcat.\, min}\right) = \frac{N_{Glycerol}^{In}\left(molmin^{-1}\right).X_G.10}{m_{catalyst}\,(g)} \quad (10)$$

where X_G is glycerol conversion to gas and y_{H_2} is the hydrogen molar fraction in gaseous products.

3. Results

3.1. Catalyst characterization

The compositions of the calcined catalysts and of the commercial catalyst are presented in Table 1. It is observed that the measured composition is similar to the desired nominal composition, considering experimental errors during preparation and also the semi-quantitative measurement of XRF analysis. The commercial catalyst also presents small amounts of magnesium and potassium oxides.

BET surface areas and pore volumes are presented in Table 1. Ni-αAl catalyst presented the lowest BET surface area, which is in accordance with literature. Pompeo *et al.* [11] have obtained a surface area of 10 m^2g^{-1} for a nickel catalyst supported on α-alumina. Ni-γAl presented the highest BET surface area and the incorporation of calcium oxide reduced BET surface area, as also observed by Dias and Assaf [12]. Adsorption-desorption isotherms of nitrogen for Ni-αAl exhibited the type II pattern, which is typical for non-porous material; on the other hand, all the other catalysts exhibited the type IV pattern, which are typical for mesoporous materials [13].

The XRD patterns of the support, calcined, reduced and spent catalysts are presented in Figure 1. In calcined catalysts, peaks related to NiO at 2θ equal to 37.3º, 43.6º and 63.3º (JCPDS 47-1049) are observed and in reduced catalysts, peaks at 44.6º, 51.8º and 76.4º (JCPDS 04-0850) related to Ni are noticed, which proves that the reduction is efficient in converting NiO species into Ni species.

In spent catalysts profiles, especially on Ni-αAl and Ni-γAl catalysts, it is possible to observe a broad peak at 26º, corresponding to a considerable amount of coke deposits formed during reaction. The peaks related to SiC are due to the difficulty of separation between the spent catalyst and the SiC used as diluent in the catalyst bed. Furthermore, the peaks related to nickel oxide are not observed on the spent

catalysts, which indicate that reduced Ni phase is stable under reaction conditions, suggesting a good interaction between nickel phase and the supports.

In Figure 1(a) sharp peaks related to α-alumina are observed in all profiles at 25.6º, 35.2º, 43.3º, 37.9º, 55.6º, 57.3º, 61.4º and 66.4º (JCPDS 10-173). In Figure 1 (b), besides the broad peaks related to γ-alumina, it is possible to notice peaks related to spinel phase ($NiAl_2O_4$) at 37.0º, 45.0º and 65.6º (JCPDS 10-339), formed due to strong interaction between nickel oxide and alumina. Spinel phase was not observed on NiCaAl catalyst profiles, showing that calcium oxide incorporation prevents the interaction between nickel and alumina, as observed by Wang and Lu [14] for $Ni/CeO_2/Al_2O_3$ catalysts.

Peaks related to calcium oxide at 2θ equal to 26.8, 32.0, 39.4 and 53.9 (JCPDS 48-1467) are shown on XRD of NiCaAl and NiCaAlcom catalysts, presented in Figures 1 (c) and (d) respectively; however, their intensities are higher on NiCaAlcom, which indicates that calcium oxide is less dispersed on this catalyst in comparison with NiCaAl. Furthermore, peaks related to a mixed oxide $(CaO)_x(Al_2O_3)_{11}$ at 2θ equal to 7.8º, 15.8º, 30.3º and 66.8º (JCPDS 41-0358) are observed on NiCaAlcom catalyst.

Table 1 shows the mean nickel crystallite size calculated before and after reaction using nickel peak at 44.5º on XRD profiles of the reduced catalysts. This Table also shows the nickel dispersion calculated by Anderson correlation. It is possible to notice that Ni-αAl presents the biggest nickel crystallite size (22.9 nm) and the lowest dispersion (4.4 %), which is in agreement with its lowest BET surface area presented in Table 1.

Furthermore, the addition of CaO on alumina support increases the nickel crystallite size and reduces considerably the dispersion in comparison with the catalyst without CaO incorporation. This behavior is in agreement with the reduction on BET surface area from 145 to 65 m^2g^{-1} with CaO incorporation, which may be covering and blocking alumina pores. It is also possible to notice that NiCaAl presents a higher nickel dispersion than NiCaAlcom.

Comparing nickel crystallite size before and after reaction, considering the analysis error, it is possible to observe similar crystallite sizes, which indicates that sintering process is not severe for these catalysts. NiCaAl catalyst presented the largest increase in crystallite size, from 15.3 to 16.8 nm, which is not very expressive.

Figure 2 shows the TPR analysis of the catalysts. Ni-γAl and Ni-αAl catalysts presented only one reduction peak centered at 800 ºC and 445 ºC, respectively. Rynkowski *et al.* [15] have reported the

existence of three different nickel species in a catalyst supported on alumina: bulk NiO, with reduction peak below 400 ºC, NiO interacting with alumina, with reduction peaks between 400 and 690 ºC, and NiO incorporated on alumina for aluminate spinel phase formation, with reduction peak above 700 ºC. Thus, it is possible to infer the existence of $NiAl_2O_4$ species on Ni-γAl catalyst, which is in agreement with XRD analysis.

Reduction profile of NiCaAl has presented one peak at 390 ºC, related to bulk NiO, four peaks between 455 ºC and 750 ºC, which are associated with NiO interacting with Al_2O_3 and CaO in different levels of interaction and one peak located at 890 ºC, related to nickel aluminate reduction. Comparing NiCaAl and Ni-γAl reduction profiles, it is possible to observe that although CaO incorporation reduces the interaction between nickel species and the support, which leads to a lower dispersion, it also reduces the formation of aluminate species, as the reduction peak located above 700 ºC is more intense and larger for Ni-γAl catalyst.

Reduction profile of NiCaAlcom catalyst has presented three overlapping peaks in the range of 500-950 ºC, the first located at 600 ºC, the second at 678 ºC and the last at 788 ºC. There is also a small peak located at 386 ºC, however the major reduction of NiO species occurs in temperatures above 400 ºC, which indicates a stronger interaction between nickel oxide and the support for NiCaAlcom catalyst.

The reduction degrees of the catalysts are presented in Table 2. Noticeably Ni-αAl presented the lowest reduction degree (54 %) in comparison with the other catalysts, which must be related with the biggest Ni crystallite size, because inner nickel oxide particles must be inaccessible for reduction with hydrogen.

TPD-NH_3 profiles of the catalysts are shown in Figure 3 and calculated acidity is presented in Table 2. The literature classifies peaks below 400 ºC as weak acid sites, while above this temperature the sites are classified as strong acid sites [16]. Thus, all the catalysts have presented mainly weak acid sites. Ni-αAl catalyst showed no NH_3 desorption peaks, therefore its acidity is zero, which can be explained by its low BET area. Ni-γAl and NiCaAl presented similar profiles, with peaks centered at 186 °C and 163°C, respectively. However, the acidity per area is higher for Ni-γAl catalyst, as also the strength of acid sites, because of the higher temperature of desorption. Thus, the addition of a basic promoter, as calcium oxide, reduced the acidity, which was also observed by Sánchez-Sánchez *et al.* [17]. NiCaAlcom catalyst presented lower acidity than NiCaAl, which can be explained by the presence of small amounts of other basic promoters as MgO and K_2O or by the different synthesis method.

3.2. Catalytic tests

Glycerol conversion and glycerol conversion to gas are presented in Figures 4 (a) and (b), respectively. Ni-αAl and Ni-γAl obtained the highest glycerol conversion in the first 8 h of reaction, with glycerol conversion in the range of 85-100 %. However they suffered a severe deactivation after 24 h of reaction. Ni-γAl conversion decayed to 67 % in 24 h of reaction and was kept constant between 67 % and 77 %; on the other hand, Ni-αAl conversion was reduced to 61% and was kept constant between 61 % and 67 %. Thus, the deactivation of Ni-αAl catalyst was more severe, which can be explained by the lowest reduction degree, lowest nickel dispersion and highest coke formation, as will be seen later for this catalyst in Figure 6. The deactivation of nickel catalysts supported on alumina has been widely reported in the literature. Sánchez *et al.* [18] have observed deactivation on Ni catalysts supported on γ- alumina after 8 h of reaction at 600 ºC and 650 ºC.

NiCaAlcom presented the lowest glycerol conversion and glycerol conversion to gas during all reaction time and also presented deactivation as glycerol conversion was reduced from 68 % in the first hour to 40 % in 24 h of reaction. This worst catalytic performance may be explained by the lower dispersion in comparison with NiCaAl and Ni-γAl; furthermore it presented lower nickel content, thus the availability of nickel species is lower for this catalyst. In contrast, NiCaAl catalyst was the only catalyst without any deactivation during reaction time: glycerol conversion was kept between 70 % and 80 % during all reaction time and was higher than glycerol conversion of Ni-γAl after 24 h of reaction.

The discrepancy between glycerol conversion and glycerol conversion to gas for all the catalyst, except for Ni-αAl, may be explained for liquid byproduct formation (acrolein, acetol and propanoic acid). Ni-αAl was the only catalyst in which the glycerol conversion and glycerol conversion to gas are almost the same during reaction time, which indicates low byproduct formation. Ni-γAl presented the highest difference in the first hours of reaction, as glycerol conversion was 98 % and glycerol conversion to gas was around 50 %; this behavior suggest not only liquid byproduct formation but also high coke formation in the first hours of reaction, which explains the fast deactivation. NiCaAl and NiCaAlcom presented similar behavior of glycerol conversion and glycerol conversion to gas, with a difference around 20 %

between both parameters, suggesting that coke formation was better distributed in reaction time, so deactivation was less severe for these catalysts in comparison with Ni-γAl catalyst.

Figures 4 (c) and (d) show hydrogen yield and hydrogen production rate during reaction time. It is possible to observe that Ni-αAl, Ni-γAl and NiCaAl showed a similar behavior, with H_2 mean yields of 37, 33 and 35 %, respectively. Hydrogen mean production rate was 4900, 4400 and 3900 μmol $H_2 g^{-1}.min^{-1}$, respectively. By the other side, NiCaAlcom has presented the lowest hydrogen mean yield (13%) and lowest hydrogen production rate, around 1600 μmol $H_2 g^{-1}.min^{-1}$. This result is associated with the lowest glycerol conversion to gas and may indicate a low activity for reforming and shift reactions.

Figures 5 (a), (b), (c) and (d) show selectivities for reforming gases: H_2, CO, CO_2 and CH_4, respectively. It is observed that Ni-αAl presented the lowest hydrogen selectivity which suggests that hydrogen generated in reforming is being consumed for coke formation by CO and CO_2 hydrogenation (Eq. 11 and 12), or by methane formation by methanation reactions (Eq. 13 and 14).

$$CO + H_2 \leftrightarrow C + H_2O \quad (11)$$

$$CO_2 + 2H_2 \leftrightarrow 2H_2O + C \quad (12)$$

$$CO + 3H_2 \leftrightarrow CH_4 + H_2O \quad (13)$$

$$CO_2 + 4H_2 \leftrightarrow CH_4 + 2H_2O \quad (14)$$

Ni-αAl showed higher selectivity to CO and lower selectivity to CO_2 than NiCaAl and Ni-γAl in the first 8 h of reaction, which indicates that shift reaction activity is low for this catalyst. Furthermore, it presented an increase in CO_2 selectivity and decrease in CO selectivity along reaction, which can be explained by CO disproportionation for coke formation as presented in Equation 15.

$$2CO \leftrightarrow CO_2 + C \quad (15)$$

NiCaAl and Ni-γAl presented a high shift reaction activity, expressed by the lowest CO and highest CO_2 selectivities, which contributes for hydrogen generation. NiCaAlcom is not very active for shift reaction, as can be seen by high CO and low CO_2 selectivities. NiCaAlcom presented the highest CO mean selectivity (25 %). For this catalyst, CO selectivity decreases from 32 % in the first hour to 7 % after 24 h of reaction.

Ni-αAl catalyst showed the highest mean methane selectivity (12 %). This high selectivity in comparison with the other catalysts is associated with the highest activity to methanation reactions, as already mentioned before, corroborating the lowest hydrogen selectivity for this catalyst.

Table 2 shows liquid byproducts yields: acrolein, acetol and propanoic acid. Acrolein and acetol are produced by glycerol dehydration (Eq. 16 and 17), and acrolein formation takes place mainly in Bronsted acid sites of the support, as it was observed by several authors [19–21]. Papageridis et al. [22] also observed the formation of liquid byproducts as acetol and acrolein employing a nickel catalyst supported on alumina for glycerol steam reforming at 500 ºC.

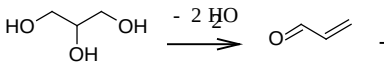

glycerol acrole (16)

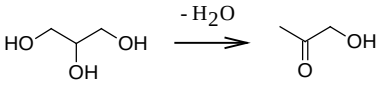

glycerol Acetol (17)

Ni-αAl catalyst showed the lowest byproduct yields, which corroborates the low difference between glycerol conversion and conversion to gas. This may be explained by its low surface area and no availability of support acid sites for byproduct formation. The mean byproduct yields for this catalyst were 0.1 % for acrolein, 2.4 % for acetol and 0.5 % for propanoic acid. On the other hand, Ni-γAl catalyst presented the highest acrolein yield in the first 8 hours of reaction, which is associated with its highest acidity. The mean acrolein yield in the first 8 h was 8.6 % and decreased for 1 % in the last 7 h of reaction, which is associated with coke formation that may cover alumina acid sites.

The catalysts with basic promoters, NiCaAl and NiCaAlcom, presented the highest acetol and propanoic acid yields during all reaction time. Propanoic acid mean yields are 10.3 % for NiCaAl and 4.1 % for NiCaAlcom; and acetol mean yields are 27.4 % for NiCaAl and 12.8 % for NiCaAlcom. Stošić et al. [23] studied the effect of acid-basic catalytic properties on glycerol dehydration and reported that, differently from acrolein formation that is favored on Bronsted acid sites, acetol yield increases with reduction in amount and strength of catalyst acid sites .

TGA and DTA analysis are presented in Figure 6. Coke formation is associated with the deactivation observed for the catalysts. Ni-αAl has showed the highest coke formation (59%), which is in

agreement with its severe deactivation. The deactivation for this catalyst is associated with its bigger nickel crystallite size, because coke formation is favored in the presence of big crystallite sizes, as observed by Lisboa et al. [24].

Coke formation on Ni-γAl, NiCaAl and NiCaAlcom is associated with acid sites presented on the catalysts, as observed by Atia et al. [25]. The incorporation of calcium oxide in NiCaAl catalyst dislocated the DTA peaks for lower temperatures, the main DTA peak for NiCaAl is located at 430 ºC and for Ni-γAl is located at 474 °C. As filamentous coke presents lower maximum oxidation temperature than amorphous coke [26, 27], this is an indication that spent NiCaAl has higher amount of filamentous coke than spent Ni-γAl. Filamentous coke is less harmful for the catalyst than amorphous coke, which corroborates the lower deactivation of NiCaAl.

4. Conclusions

Three nickel catalysts, supported on alpha alumina (Ni-αAl), gama alumina (Ni-γAl) and CaO/γ-Al_2O_3 (NiCaAl) were synthesized by wet impregnation of nickel precursors on supports and evaluated in glycerol steam reforming at 500 ºC, during 30 h. A fourth commercial catalyst (NiCaAlcom) for methane steam reforming was also evaluated in glycerol steam reforming. NiCaAl catalyst was the only catalyst that did not present any deactivation during all reaction time, with glycerol conversion to gas of approximately 55 % and hydrogen yield of approximately 35 %. The addition of calcium oxide decreased the BET surface area and nickel dispersion, and reduced the catalyst acidity and acid strength, properties related with coke formation. Besides, it reduced nickel aluminate formation, decreasing the reduction temperature. Beyond that, the type of coke was modified by calcium oxide addition; for NiCaAl catalyst coke formed was mainly in filamentous form and for Ni-γAl the coke was mainly amorphous, which explained the deactivation for Ni-γAl and non-deactivation for NiCaAl.

Ni-αAl catalyst presented the lowest BET surface area, nickel dispersion and its acidity was zero. This catalyst suffered severe deactivation mainly by coke formation, as shown by TG analysis. The consumption of hydrogen for coke and methane formation explained the lowest hydrogen selectivity for this catalyst. NiCaAlcom catalyst presented the worst catalytic performance in terms of glycerol conversion, conversion to gas and hydrogen production, with low activity for shift reaction.

In terms of liquid byproduct formation, calcium oxide addition reduced acrolein formation but increased acetol and propanoic formation in comparison with Ni-γAl catalyst. On the other hand, Ni-αAl catalyst presented insignificant liquid byproduct formation, explained by its lowest BET area and acidity.

Acknowledgements

The authors thank FAPERJ, CNPq, and CAPES for financial support granted to carry out this work, and Greentec/EQ/UFRJ for N_2 adsorption analyses.

References

1. Shahid, E.M., Jamal, Y.: A review of biodiesel as vehicular fuel. Renew. Sustain. Energy Rev. 12, 2477–2487 (2008). doi:10.1016/j.rser.2007.06.001

2. Adhikari, S., Fernando, S.D., To, S.D.F., Bricka, R.M., Steele, P.H., Haryanto, A.: Conversion of glycerol to hydrogen via a steam reforming process over nickel catalysts. Energy and Fuels. 22, 1220–1226 (2008). doi:10.1021/ef700520f

3. Balat, H., Kirtay, E.: Hydrogen from biomass - Present scenario and future prospects. Int. J. Hydrogen Energy. 35, 7416–7426 (2010). doi:10.1016/j.ijhydene.2010.04.137

4. Wang, C., Dou, B., Chen, H., Song, Y., Xu, Y., Du, X., Luo, T., Tan, C.: Hydrogen production from steam reforming of glycerol by Ni-Mg-Al based catalysts in a fixed-bed reactor. Chem. Eng. J. 220, 133–142 (2013). doi:10.1016/j.cej.2013.01.050

5. Silva, J.M., Soria, M.A., Madeira, L.M.: Challenges and strategies for optimization of glycerol steam reforming process. Renew. Sustain. Energy Rev. 42, 1187–1213 (2015). doi:10.1016/j.rser.2014.10.084

6. Cortright, R.D., Davda, R.R., Dumesic, J.A.: Hydrogen from catalytic reforming of biomass-derived hydrocarbons in liquid water. Nature. 418, 964–967 (2002). doi:10.1038/nature01009

7. Davda, R.R., Shabaker, J.W., Huber, G.W., Cortright, R.D., Dumesic, J.A.: A review of catalytic issues and process conditions for renewable hydrogen and alkanes by aqueous-phase reforming of oxygenated hydrocarbons over supported metal catalysts. Appl. Catal. B Environ. 56, 171–186 (2005). doi:10.1016/j.apcatb.2004.04.027

8. Shabaker, J.W., Huber, G.W., Dumesic, J.A.: Aqueous-phase reforming of oxygenated hydrocarbons over Sn-modified Ni catalysts. J. Catal. 222, 180–191 (2004). doi:10.1016/j.jcat.2003.10.022

9. Shabaker, J.W., Davda, R.R., Huber, G.W., Cortright, R.D., Dumesic, J.A.: Aqueous-phase reforming of methanol and ethylene glycol over alumina-supported platinum catalysts. J. Catal. 215, 344–352 (2003). doi:10.1016/S0021-9517(03)00032-0

10. Anderson, J.R.: Structure of Metallic Catalysts. Academic Press, London (1975)

11. Pompeo, F., Nichio, N.N., Ferretti, O.A., Resasco, D.: Study of Ni catalysts on different supports to obtain synthesis gas. Int. J. Hydrogen Energy. 30, 1399–1405 (2005). doi:10.1016/j.ijhydene.2004.10.004

12. Dias, J.A.C., Assaf, J.M.: Influence of calcium content in Ni/CaO/γ-Al_2O_3 catalysts for CO_2-reforming of methane. Catal. Today. 85, 59–68 (2003). doi:10.1016/S0920-5861(03)00194-9

13. Sing, K.S.W.: Reporting physisorption data for gas/solid systems with special reference to the determination of surface area and porosity (Recommendations 1984). Pure Appl. Chem. 57, 603–619 (1985). doi:10.1351/pac198557040603

14. Wang, S., Lu, G.Q.M.: Role of CeO_2 in Ni / CeO_2 ± Al_2O_3 catalysts for carbon dioxide reforming of methane. 19, 7435–7443 (1998). doi:10.1016/S1004-9541(14)60029-X

15. Rynkowski, J.M., Paryjczak, T., Lenik, M.: On the nature of oxidic nickel phases in NiO/γ-Al_2O_3 catalysts. Appl. Catal. A, Gen. 106, 73–82 (1993). doi:10.1016/0926-860X(93)80156-K

16. Ribeiro, N.F.P., Henriques, C.A., Schmal, M.: Copper-based catalysts for synthesis of methylamines: The effect of the metal and the role of the support. Catal. Letters. 104, 111–119 (2005). doi:10.1007/s10562-005-7939-7

17. Sánchez-Sánchez, M.C., Navarro, R.M., Fierro, J.L.G.: Ethanol steam reforming over Ni / MxOy-Al_2O_3 (M = Ce, La, Zr and Mg) catalysts: Influence of support on the hydrogen production. Int. J. Hydrogen Energy. 32, 1462–1471 (2007). doi:10.1016/j.ijhydene.2006.10.025

18. Sánchez, E.A., D'Angelo, M.A., Comelli, R.A.: Hydrogen production from glycerol on Ni/Al_2O_3

catalyst. Int. J. Hydrogen Energy. 35, 5902–5907 (2010). doi:10.1016/j.ijhydene.2009.12.115

19. Manfro, R.L., Pires, T.P.M.D., Ribeiro, N.F.P., Souza, M.M.V.M.: Aqueous-phase reforming of glycerol using Ni–Cu catalysts prepared from hydrotalcite-like precursors. Catal. Sci. Technol. 3, 1278 (2013). doi:10.1039/c3cy20770f

20. Haider, M.H., Dummer, N.F., Zhang, D., Miedziak, P., Davies, T.E., Taylor, S.H., Willock, D.J., Knight, D.W., Chadwick, D., Hutchings, G.J.: Rubidium- and caesium-doped silicotungstic acid catalysts supported on alumina for the catalytic dehydration of glycerol to acrolein. J. Catal. 286, 206–213 (2012). doi:10.1016/j.jcat.2011.11.004

21. Atia, H., Armbruster, U., Martin, A.: Influence of alkaline metal on performance of supported silicotungstic acid catalysts in glycerol dehydration towards acrolein. Appl. Catal. A Gen. 393, 331–339 (2011). doi:10.1016/j.apcata.2010.12.015

22. Papageridis, K.N., Siakavelas, G., Charisiou, N.D., Avraam, D.G., Tzounis, L., Kousi, K., Goula, M.A.: Comparative study of Ni, Co, Cu supported on γ-alumina catalysts for hydrogen production via the glycerol steam reforming reaction. Fuel Process. Technol. 152, 156–175 (2016). doi:10.1016/j.fuproc.2016.06.024

23. Stošić, D., Bennici, S., Sirotin, S., Calais, C., Couturier, J.L., Dubois, J.L., Travert, A., Auroux, A.: Glycerol dehydration over calcium phosphate catalysts: Effect of acidic-basic features on catalytic performance. Appl. Catal. A Gen. 447–448, 124–134 (2012). doi:10.1016/j.apcata.2012.09.029

24. Lisboa, J.D.S., Santos, D.C.R.M., Passos, F.B., Noronha, F.B.: Influence of the addition of promoters to steam reforming catalysts. Catal. Today. 101, 15–21 (2005). doi:10.1016/j.cattod.2004.12.005

25. Atia, H., Armbruster, U., Martin, A.: Influence of alkaline metal on performance of supported silicotungstic acid catalysts in glycerol dehydration towards acrolein. Appl. Catal. A Gen. 393, 331–339 (2011). doi:10.1016/j.apcata.2010.12.015

26. Quitete, C.P.B., Bittencourt, R.C.P., Souza, M.M.V.M.: Coking resistance evaluation of tar removal catalysts. Catal. Commun. 71, 79–83 (2015). doi:10.1016/j.catcom.2015.08.013

27. Jackson, S.D., Thomson, S.J., Webb, G.: Carbonaceous deposition associated with the catalytic steam-reforming of hydrocarbons over nickel alumina catalysts. J. Catal. 70, 249–263 (1981). doi:10.1016/0021-9517(81)90338-9

Table 1. Chemical composition of the catalysts, nickel crystallite size and dispersion before[a] and after[b] reaction, BET surface area and pore volume of calcined catalysts.

Catalyst	wt% NiO	wt% CaO	wt% MgO	wt% K_2O	Ni crystallite size[a] (nm)	Ni crystallite size[b] (nm)	D^a (%)	D^b (%)	S_{BET} (m^2g^{-1})	V_{Pore} (cm^3g^{-1})
Ni-αAl	26	0	0	0	22.9 ± 0.8	23.3 ± 3.8	4.4	4.3	12	0.03
Ni-γAl	21	0	0	0	8.4 ± 2.0	8.4 ± 0.7	12.0	12.0	145	0.34
NiCaAl	25	12	0	0	15.3 ± 1.2	16.8 ± 1.5	6.6	6.0	65	0.38
NiCaAlcom	15	14	1	2	18.2 ± 1.0	16.2 ± 1.1	5.5	6.2	88	0.13

Table 2. Reduction degree (RD) of NiO calculated from TPR results, amount of desorbed NH_3 per mass and per BET area calculated from TPD results, and acrolein (Y_{acr}) , acetol (Y_{ace}) and propanoic acid (Y_{acp}) average yields.

Catalyst	RD (%)	μmol NH_3 $gcat^{-1}$	μmol NH_3 m^{-2}	Y_{acr} (1-8 h)	Y_{acr} (24-30 h)	Y_{ace} (1-8h)	Y_{ace} (24-30h)	Y_{acp} (1-8h)	Y_{acp} (24-30h)
Ni-αAl	54	0.0	0.0	0.1	0.1	2.2	2.6	0.4	0.6
Ni-γAl	90	458.9	3.1	7.6	1.0	6.7	2.3	2.7	0.7
NiCaAl	99	105.4	1.6	5.9	6.0	28.4	26.2	11.6	8.8
NiCaAlcom	100	24.1	0.3	3.5	3.6	12.4	13.2	4.3	3.9

Figure captions

Figure 1. XRD patterns of Ni-αAl (a), Ni-γAl (b), NiCaAl (c) and NiCaAlcom (d) catalysts.

Figure 2.TPR profiles of the calcined catalysts.

Figure 3. TPD-NH_3 profiles of the reduced catalysts.

Figure 4. Glycerol conversion (a), glycerol conversion into gas (b), H_2 yield (c) and hydrogen production rate (d) for the catalysts during glycerol steam reforming. Reaction conditions: 500 ^{o}C, GHSV of 200,000 h^{-1} and 20 % v/v glycerol solution.

Figure 5. Selectivities to H_2 (a), CO (b), CO_2 (c) and CH_4 (d) for the catalysts during glycerol steam reforming. Reaction conditions: 500 ^{o}C, GHSV of 200,000 h^{-1} and 20 % v/v glycerol solution.

Figure 6. TGA and DTA of the spent catalysts.

Figure 1

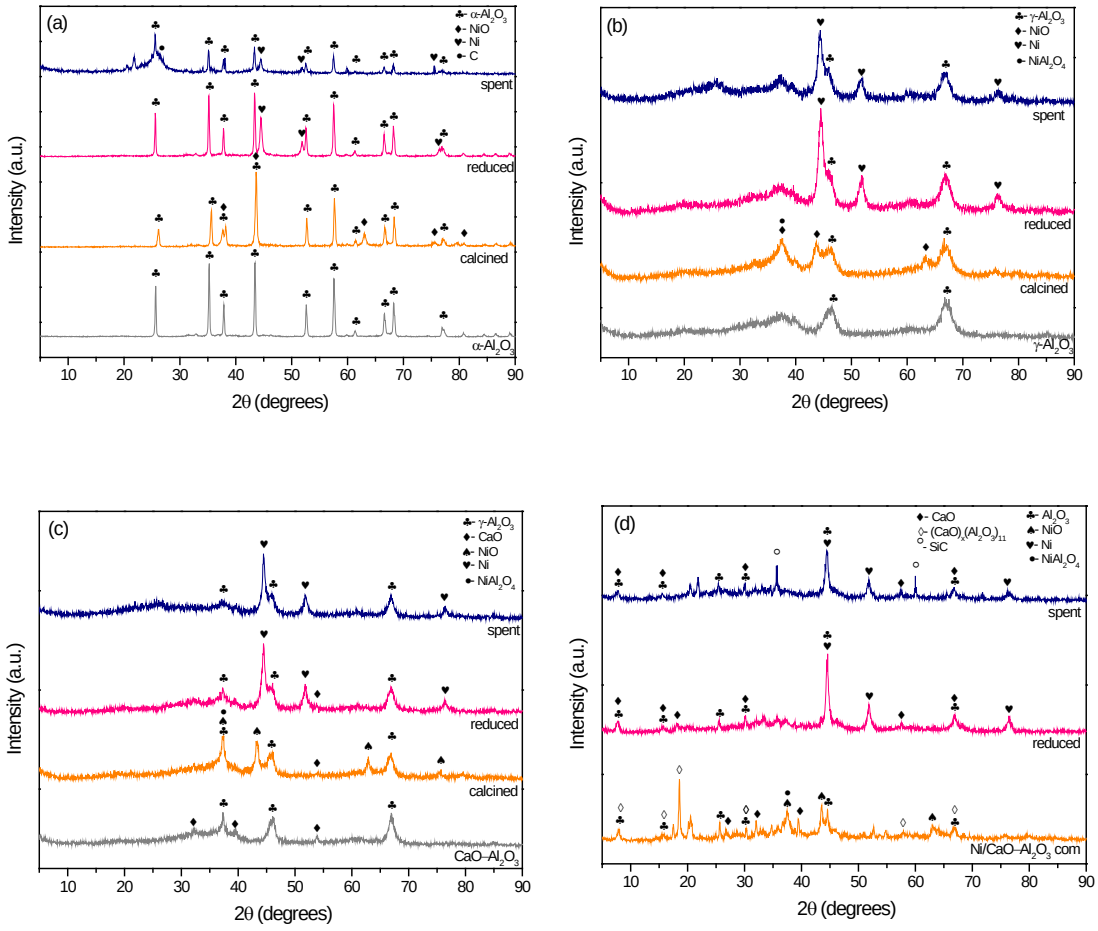
(a)
♣- α-Al2O3
♦- NiO
♥- Ni
●- C
spent
reduced
calcined
α-Al2O3
Intensity (a.u.)
2θ (degrees)
(b)
♣- γ-Al2O3
♦- NiO
♥- Ni
●- NiAl2O4
spent
reduced
calcined
γ-Al2O3
Intensity (a.u.)
2θ (degrees)
(c)
♣- γ-Al2O3
♦- CaO
♣- NiO
♥- Ni
●- NiAl2O4
spent
reduced
calcined
CaO–Al2O3
Intensity (a.u.)
2θ (degrees)
(d)
♦- CaO
◊- (CaO)x(Al2O3)11
○- SiC
♣- Al2O3
♣- NiO
♥- Ni
●- NiAl2O4
spent
reduced
Ni/CaO–Al2O3 com
Intensity (a.u.)
2θ (degrees)

Figure 2

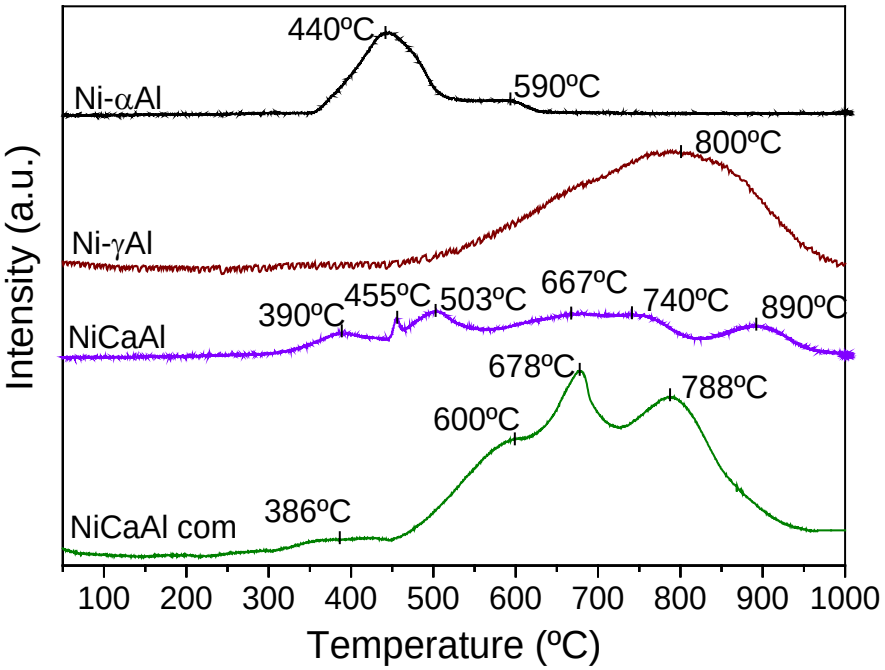
440ºC
590ºC
Ni-αAl
800ºC
Ni-γAl
390ºC
455ºC
503ºC
667ºC
740ºC
890ºC
NiCaAl
678ºC
788ºC
600ºC
386ºC
NiCaAl com
Intensity (a.u.)
100
200
300
400
500
600
700
800
900
1000
Temperature (ºC)

Figure 3

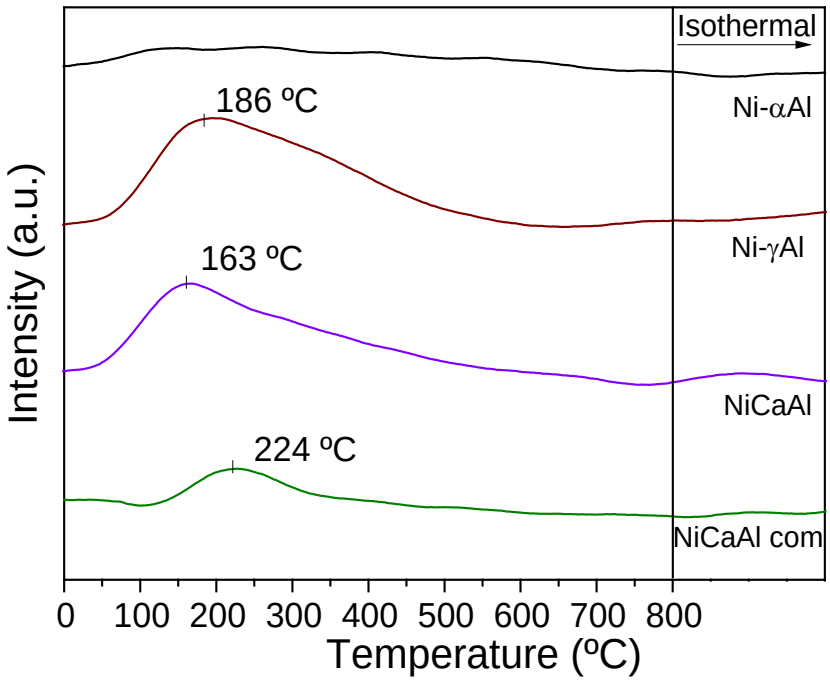
Isothermal
186 ºC
Ni-αAl
Ni-γAl
163 ºC
NiCaAl
224 ºC
NiCaAl com
Intensity (a.u.)
0 100 200 300 400 500 600 700 800
Temperature (ºC)

Figure 4

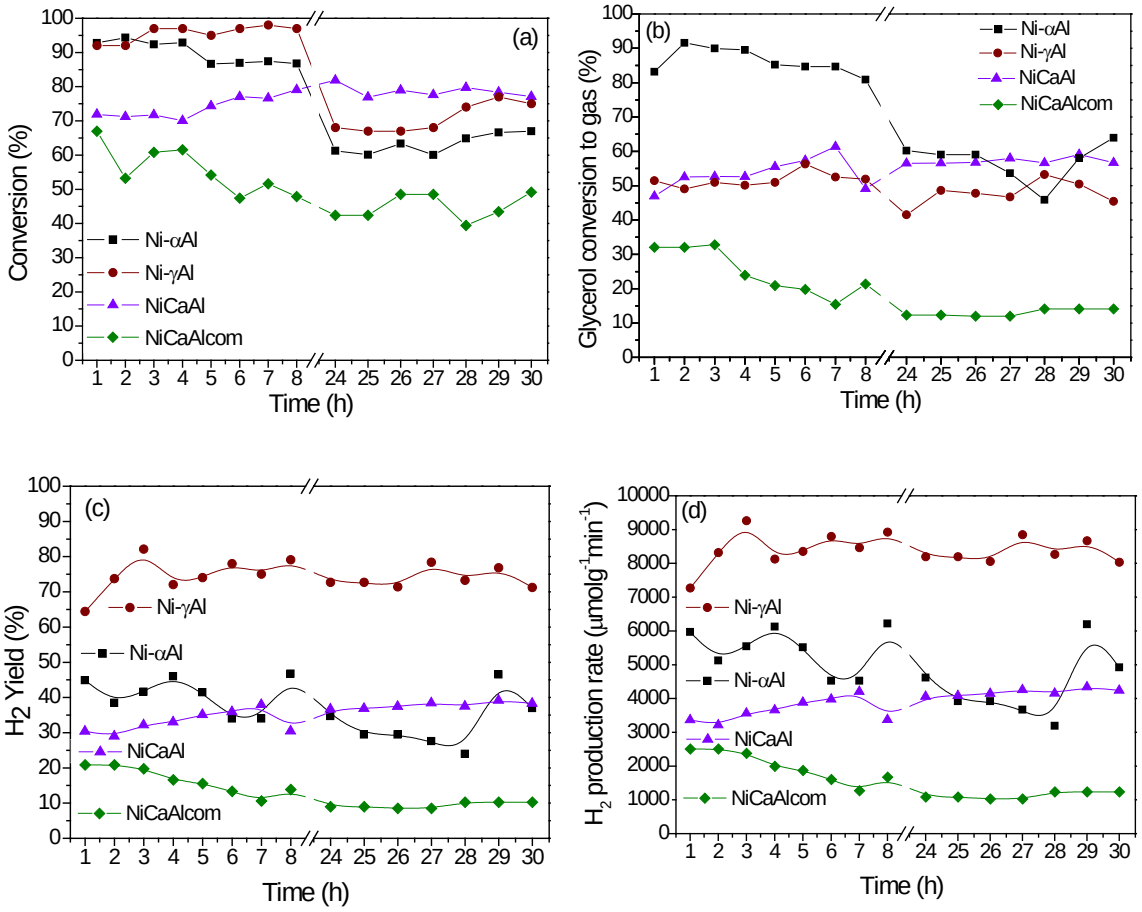
(a)
Conversion (%)
Time (h)
Ni-αAl
Ni-γAl
NiCaAl
NiCaAlcom
(b)
Glycerol conversion to gas (%)
Time (h)
Ni-αAl
Ni-γAl
NiCaAl
NiCaAlcom
(c)
H2 Yield (%)
Time (h)
Ni-γAl
Ni-αAl
NiCaAl
NiCaAlcom
(d)
H2 production rate (μmolg-1min-1)
Time (h)
Ni-γAl
Ni-αAl
NiCaAl
NiCaAlcom

Figure 5

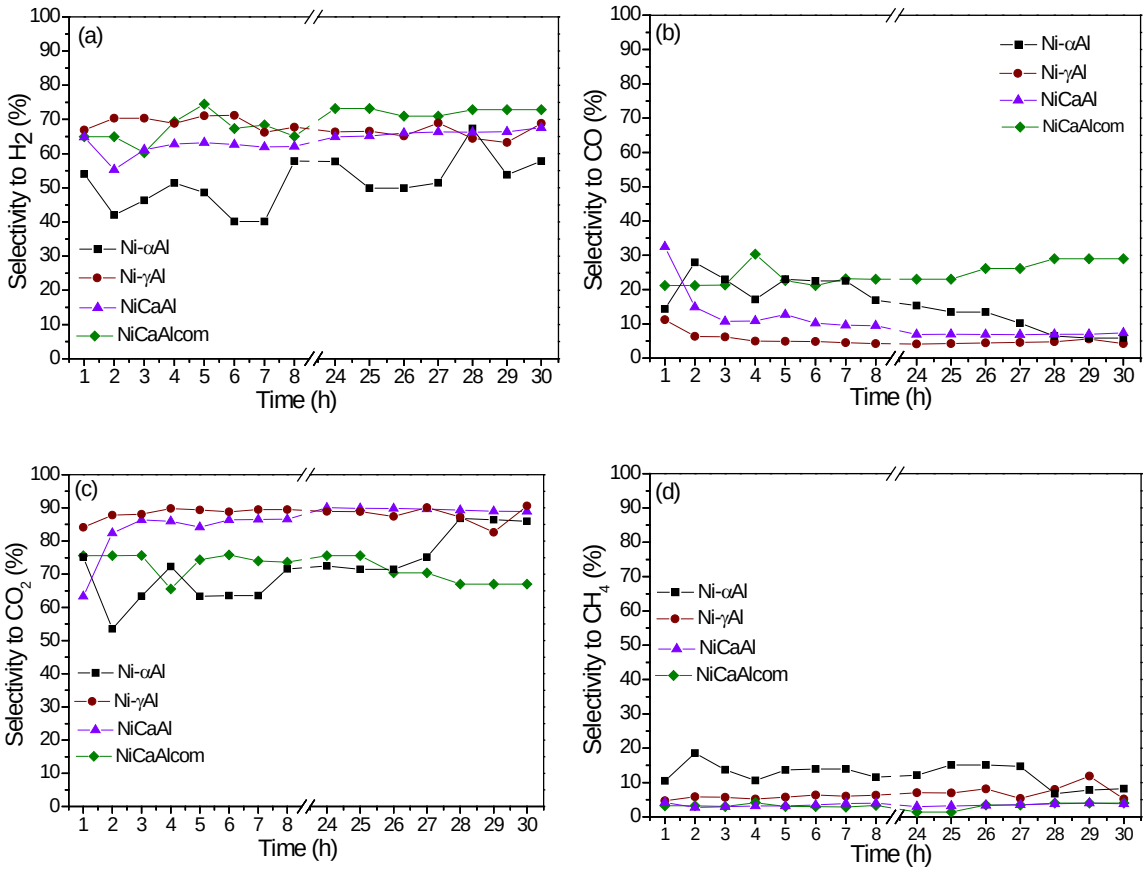
(a)
Selectivity to H_2 (%)
Time (h)
Ni-αAl
Ni-γAl
NiCaAl
NiCaAlcom
(b)
Selectivity to CO (%)
Time (h)
(c)
Selectivity to CO_2 (%)
Time (h)
(d)
Selectivity to CH_4 (%)
Time (h)

Figure 6

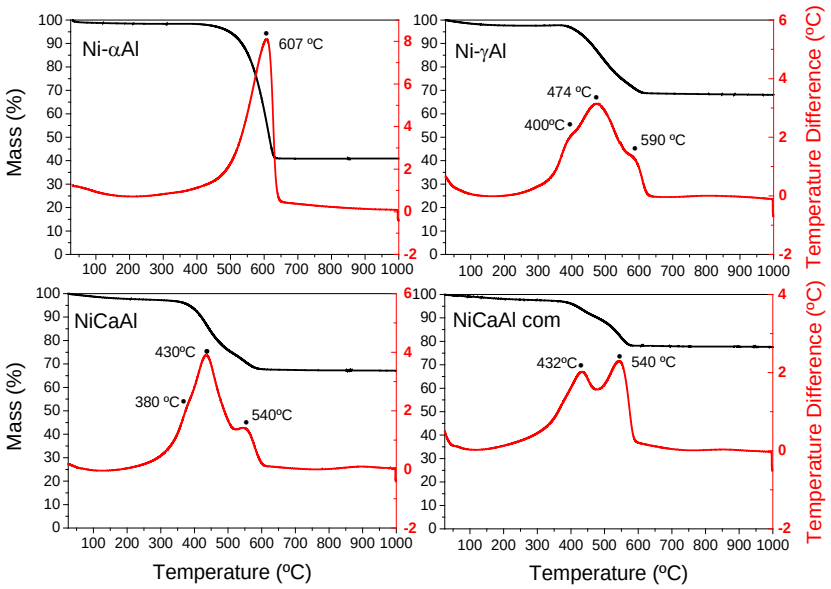
Ni-αAl
607 ºC
Ni-γAl
474 ºC
400ºC
590 ºC
NiCaAl
430ºC
380 ºC
540ºC
NiCaAl com
432ºC
540 ºC
Mass (%)
Temperature Difference (ºC)
Temperature (ºC)